ASSOCIAZIONE NAZIONALE ITALIANA DI INGEGNERIA SISMICA
ANIDIS
Italian National Association of Earthquake Engineering

XVIII CONVEGNO ANIDIS
L'ingegneria sismica in Italia
ASCOLI PICENO 2019
15-19 Settembre

Recent results on the use of smart bricks for earthquake-induced damage detection in masonry structures

Antonella D'Alessandro[a], Andrea Meoni[a], Filippo Ubertini[a]
[a] *Department of Civil and Environmental Engineering, University of Perugia, via G. Duranti 93, 06125, Perugia, Italy*

Keywords: smart bricks, monitoring of masonry structures, strain field reconstruction, numerical simulation, damage detection.

ABSTRACT
The paper presents the recent results of an ongoing research project carried out at the Department of Civil and Environmental Engineering of University of Perugia, entitled "Smart Bricks", about the monitoring of masonry structures by use of novel strain-sensitive burned clay-based sensors. The Authors propose and investigate a modified composite structural brick, composed by a clay matrix with inclusions of stainless steel microfibers, able to identify changes in mechanical strain and, consequently, to monitor the masonry where it is integrated. Experimental compressive tests on single bricks, with different amounts of filler, demonstrate their sensitivity to external applied strains and stresses, and permit to identify the most performing composition. The smart bricks were then included in small-scale and medium-scale walls and subjected to different loading conditions for investigating the sensitivity of the new sensors to changes in load path and to the development of cracks. Numerical simulations were conducted in order to analyze the optimal smart-brick configuration for the detection of changes in the strain field and the load path of the masonry. Numerical and experimental results were compared to validate the smart bricks' capabilities for strain field reconstruction and damage detection.

1 INTRODUCTION

The monitoring of the service performance interests all types of structures and infrastructures, due to its safety implications (Carpinteri et al. 2006; Mosquera et al. 2012). The control of strategic constructions and existing buildings result particularly significant because of the presence of users and the possible degradation of materials and elements (De Lorenzis et al. 2007; Laflamme et al. 2015). Critical events, as earthquakes, can compromise the integrity of the structures and cause dangerous cracks, damages and collapses, so a quick detection of the behavior is desirable (Saisi et al. 2014; Masciotta et al. 2017). Among all the construction typologies, masonry structures appear particularly affected by seismic loads because they exhibit a brittle failure mechanism and a non-homogeneous behavior (Formisano et al. 2018; Meoni et al. 2019). So, a diffuse monitoring of these constructions during their service life results essential for the identification of critical modifications of the structural behavior.

Traditional Structural Health Monitoring (SHM) systems use commercial sensors deployed in a limited number of points and may not be able to detect local modifications or crack developments. Moreover, such sensors are externally attached, possess physical and mechanical properties very different from those of the structure they monitor and show issues about durability, costs of placement and maintenance. Recently, the development of materials' science determined the availability of different types of multifunctional construction materials, with enhanced physical, chemical, electrical and mechanical properties (Pisello et al. 2017). In particular, the addition of piezoresistive fillers can enhance the self-sensing capabilities of the matrix they are dispersed in (Coppola et al. 2011, Rainieri et al. 2013; Han et al. 2015). Such modified materials have durability similar to the original matrices, lower costs, an extensive and easier applicability.

The Authors started a research about smart clay bricks doped with stainless steel microfibers, extending the approach developed for composite

cement-based materials (D'Alessandro et al. 2018; Downey et al. 2017; Garcia-Macias et al. 2017). This paper presents the preparation procedure of the smart bricks proposed by the Authors and the electromechanical tests carried out on single bricks, small-scale and medium-scale walls with smart bricks to investigate their sensing capabilities. The experimental results have been compared with those from numerical simulations, in order to validate the smart bricks' capabilities of strain field reconstruction and damage detection.

2 MATERIALS AND METHODS

2.1 Smart bricks production

Smart bricks with prismatic nominal shape of 70x50x50 mm^3 were produced by considering the manufacturing procedure reported in Fig. 1.

Fresh clay was mechanically mixed with conductive stainless steel micro-fibers, model R.STAT/S, added in various percentages, from 0% to 1% with respect to the weight of the clay (Fig. 1 (A)).

Samples were first formed by pouring the composite material (Fig. 1(B)) into prismatic oiled molds sprinkled with sand and then dried up to 90°C and burned by performing a thermal cycle up to 900°C (Fig. 1(C)). Afterwards, each specimen was instrumented by applying two external copper plate electrodes on its opposite sides, covering them with an insulating layer (Fig. 1 (D)).

2.2 Electrical measurements

Electrical measurements were performed by applying a biphasic DC measurements approach where the input was a voltage square wave with an amplitude of ±10 V (20 V peak-to-peak), 50% of duty cycle and frequency of 1Hz, by using a function generator, model RIGOL DG1022.

The output was a current signal acquired by using a DAQ NI PXIe-1073 equipped with a digital multimeter, model NI PXI-4071, at a sampling frequency of 10Hz (Downey et al. 2017). Electrical resistance was computed according to the Ohm's law by considering the current intensity measurement taken at the 80% of the positive constant part of the acquired output signal:

$$R(t)|_{t=\hat{t}} = V/I(t)|_{t=\hat{t}}, \qquad (1)$$

where, V is the applied positive constant voltage, equal to +10V, I is the measured current intensity and $\hat{t}$ is the time instant when the sample is taken.

3 EXPERIMENTAL TESTS

3.1 Single smart bricks with different percentages of fibers

Electromechanical tests were performed on single smart bricks by applying the uniaxial cyclical compression load history reported in Fig. 2(a), in order to investigate their strain-sensing capability varying the amount of conductive filler present inside the clay matrices.

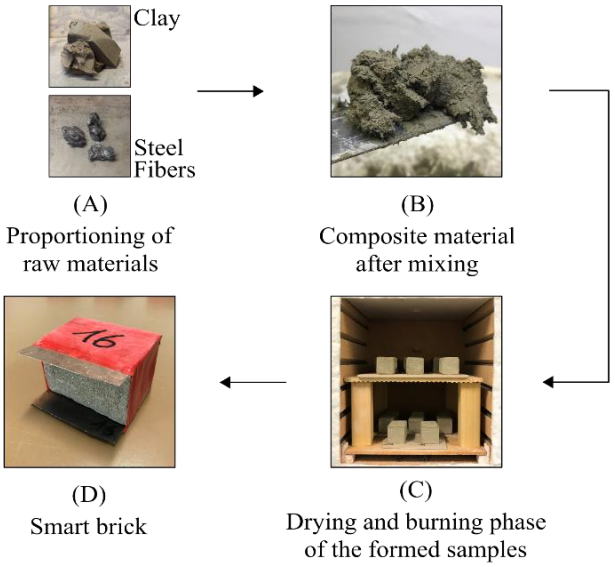

Figure 1. Smart brick production procedure.

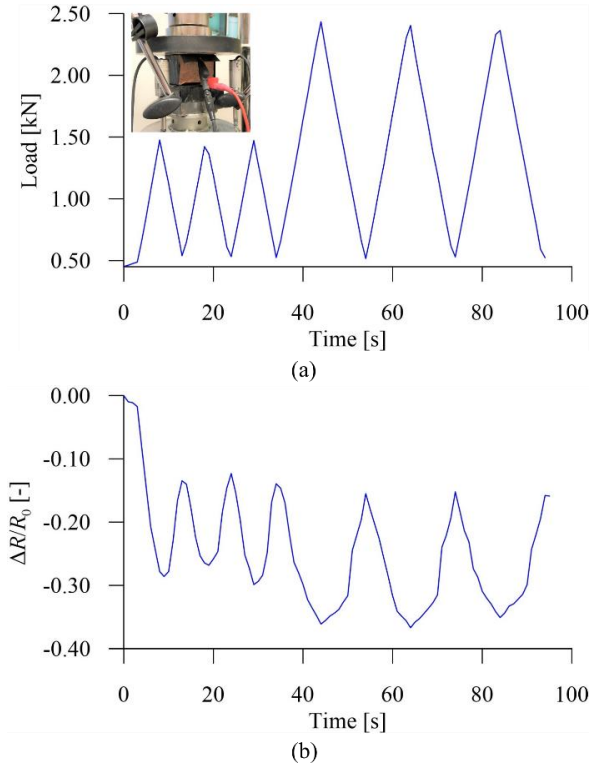

Figure 2. Electromechanical tests on single smart bricks: (a) Applied load history and a detail view of a instrumented sample during the tests; (b) Example of normalized change in electrical resistance measured by the smart brick made with the 0.25% of stainless steel filler.

Smart bricks were able to detect the applied load and its variation over the time as demonstrated in Fig. 2(b), where an example of the normalized change in electrical resistance measured by the smart brick made with the 0.25% of stainless steel filler is reported.

Fig. 3 depicts results obtained from each smart brick by comparing its normalized change in electrical resistance versus the strain of the samples estimated through displacement measurements obtained from three linear variable differential transformers (LVDTs) placed at 120°.

Data were fitted with linear regression and the quality of the sensor's response was assessed by considering the value of the determination coefficient, R^2.

Results show that the addition of stainless steel micro-fibers to the clay matrices enhances their strain-sensing capability also improving the linearity of the response of the doped sensors with respect to the normal sample.

Electromechanical tests on small-scale walls were performed in order to deepen the investigation on the smart bricks' behavior when embedded into masonry structures. To this aim, previously tested smart bricks were placed at the middle of a small-scale wall, of 145x50x160 mm^3, composed of three rows, and subjected to an uniaxial cyclical compression load history reported in Fig. 4(a).

3.2 Small-scale walls with bricks of different percentages of fibers

An example of normalized change in electrical resistance measured by the embedded smart brick made with the 0.25% of stainless steel filler is reported in Fig. 4(b).

Data obtained from each test were fitted with linear regression and plotted in Fig. 5, also reporting the value of the determination coefficient, R^2, in order to evaluate the sensor's response. As before, the plot depicts the comparison between the normalized change in electrical resistance, measured by each smart brick, versus the strain output measured as explained before from LVDTs' data. Reported results show that the smart bricks doped with 0.25% of stainless steel micro-fibers are characterized by a higher strain-sensing capability than that of the other ones.

Moreover, considering the linear response, the brick with 0.25% of conductive filler appeared the most suitable sensor to be embedded within a middle-scale wall.

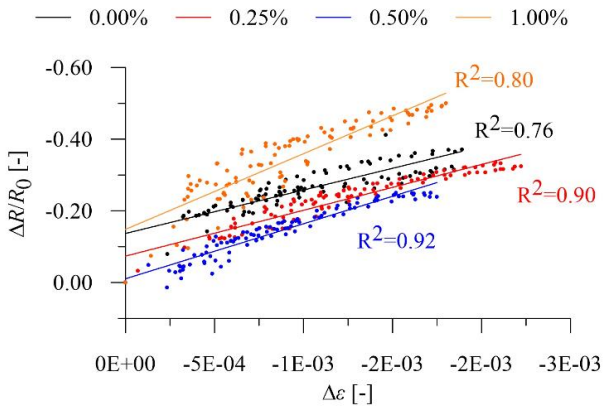

Figure 3. Normalized change in electrical resistance versus strain from electromechanical tests on single smart bricks with different percentage of stainless steel filler.

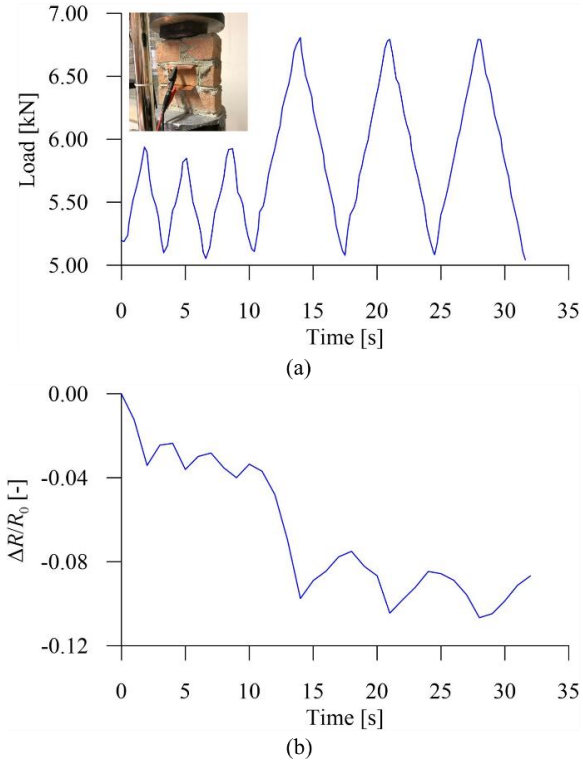

Figure 4. Electromechanical tests on small-scale walls: (a) applied load history and a detail view of a sample during the tests; (b) normalized change in electrical resistance of the the embedded smart brick made with the 0.25% of filler.

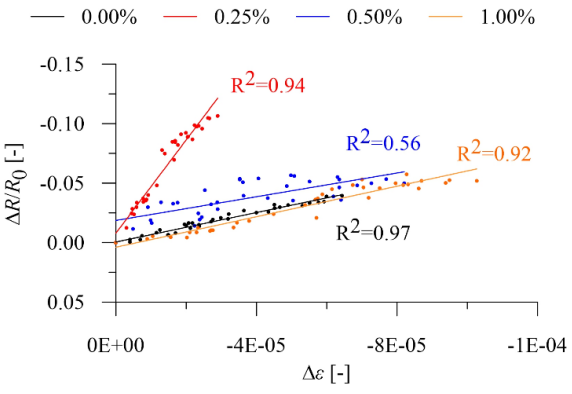

Figure 5. Normalized change in electrical resistance versus strain obtained from electromechanical tests on small-scale walls.

3.3 *Middle-scale wall with bricks doped with 0.25% of steel microfibers*

In order to investigate the effectiveness of smart bricks to monitor changes in axial strain and to reconstruct strain field maps when embedded into masonry structural elements, electromechanical tests were performed on a middle-scale wall of 375x50x385 mm^3, made of bricks arranged in seven rows equipped with seven 0.25% smart bricks, by applying an eccentric axial compression load on the right side of the wall characterized by a load history reported in Fig. 6. The smart bricks' deployment was reported in Fig. 7(a) as well as the cracking pattern that interested the wall during the tests, due to the application of an eccentric axial compression load, of 30kN, applied on the left side of the wall in the first part of the experimental campaign. The application of the eccentric compression loads on the right side of the wall did not produce any visible new cracks but only the increase in the existing openings. Fig. 7(b) shows the variations in axial strain estimated from each smart brick versus the maximum values of the changes in stress computed for each load step respect to the initial load of 5kN. Stress conditions were computed considering, at a first level of approximation, a linear elastic beam model, where the developing of the cracks in tension was considered by neglecting the tensile strength of masonry, so taking into account a partialized cross-section of the wall (Downey et al. 2017).

Considering a step *s* of the applied load history, the variations in axial strain, $\Delta\varepsilon$, for the *i*-th smart brick were computed considering the following equation:

$$\Delta\varepsilon_i^s = -\frac{1}{\lambda_i}\frac{R_i^s - R_i^0}{R_i^0}, \qquad (2)$$

where, R_i^s is the electrical resistance measured at the considered step of the load history, R_i^0 is the value of electrical resistance measured after the application of the initial load of 5kN and λ_i is the gauge factor estimated during electromechanical tests performed on each single smart brick before its embedding.

Results reported in Fig. 7(b) show that smart bricks E and G placed in the right part of the wall are the most stressed/deformed sensors and their variations in axial strain grows with respect to the increase of the load. Smart bricks H and F, on the left side of the wall, show a less marked variation in axial strain after the execution of the load range 5kN-25kN, due to the increase in existing cracks openings that contributes to deviate the load paths on the right side of the wall.

The non-linear trend shown by the variations in axial strain of the smart brick A after the execution of the load range 5kN-15kN, could also be associated to an increase in cracks openings.

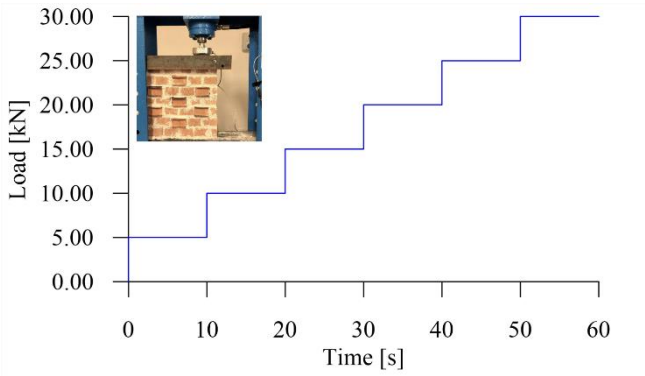

Figure 6. Load history applied during electromechanical tests on middle-scale wall on the left side of the sample.

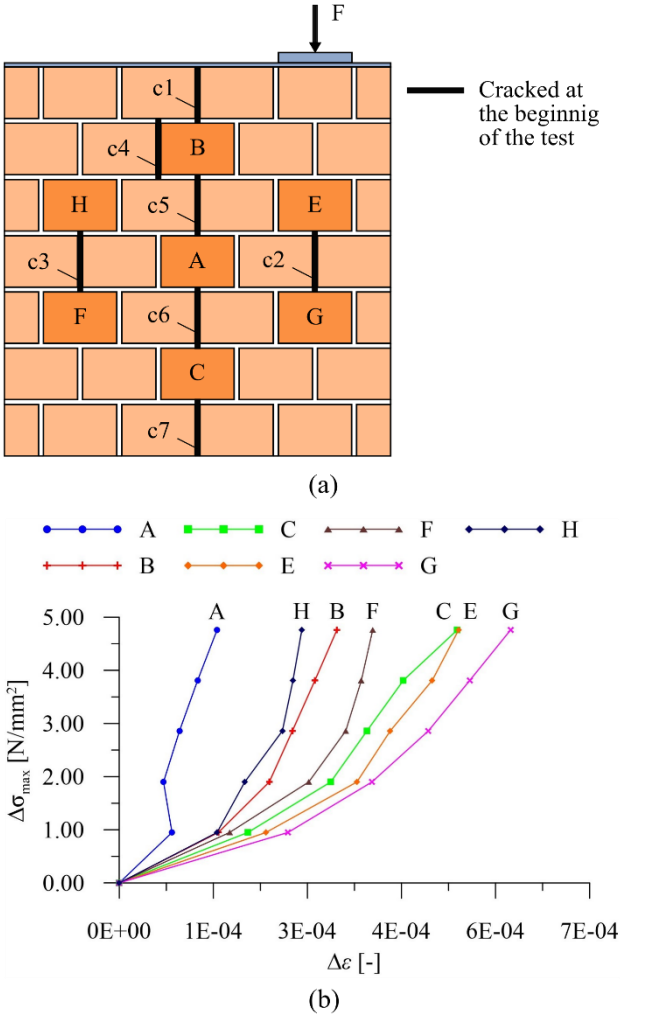

Figure 7. Results from electromechanical tests on middle-scale wall: (a) Smart bricks deployment and detected cracking pattern; (b) Trends of variation in axial strain for each load range estimated from smart bricks' outputs.

3.4 Numerical simulations

In order to numerically reconstruct the strain field maps, a commonly used technique of interpolation for spatial data, ordinary kriging, was employed to predict values of the variations in axial strain on the middle-scale wall, taking into account those experimentally estimated from the embedded smart bricks as training data (Cressie 1988).

It is worth noting that in this work a linear variogram was considered to model the spatial correlation in the random space between point pairs. Fig. 8(a) reports an example of strain field map reconstructed for the last load range, 5kN-30kN.

Numerical results, which point out an area with an high concentration of strain on the right side of the wall and an area, close to the left upper corner of the wall, where the concentration of the strain is low, are consistent with the experimental ones, suggesting that data obtained from smart bricks may be used for strain map reconstruction.

Moreover, kriging interpolation was also used in order to understand what kind of information it is possible to obtain from reconstructing strain field maps by decreasing the number of smart bricks employed in the simulations. Results obtained for the load range 5kN-30kN are reported in Fig. 8(b, c, d). Mean Absolute Error (MAE) was computed for each case, with respect to the strain field map numerically estimated by considering the data from all the seven embedded smart bricks. Results are reported in Fig. 9.

Overall in terms of accuracy, the maximum value of the MAE, obtained for the strain field map predicted with three smart bricks, is almost an order of magnitude lower than the estimated variations in axial strain and thus can be considered acceptable even if it tends to underestimate the predictions.

On the other hand, examples depicted in Fig. 8 show that limiting the number of smart bricks considered in the kriging simulations leads to miss some local information regarding the load paths distribution even if, in this example, the strain field map reconstructed by considering data from only four smart bricks can be considered consistent and comparable with the obtained experimental results.

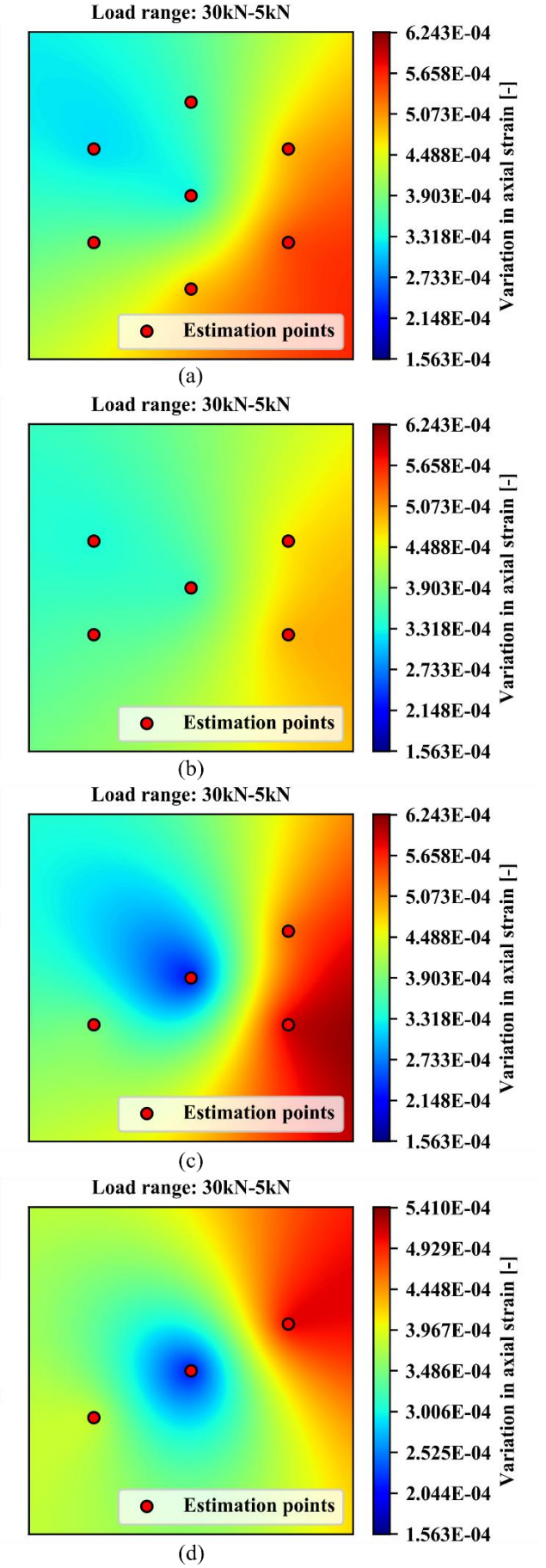

Figure 8. Strain filed maps reconstructed by varying the number of the smart bricks employed.

4 CONCLUSION

The paper has presented results obtained from the characterization of the behavior of smart bricks, made with different amount of conductive filler of stainless steel microfibers. Tests concerned single bricks, small-scale and medium-scale walls. Results from electromechanical tests performed on a middle-scale wall with smart bricks were used to monitor variations in axial strain, and the effectiveness of data outputted by smart bricks to reconstruct strain field maps using a spatial interpolation method was evaluated.

Electromechanical tests on single smart bricks demonstrated that the addition of stainless steel micro-fibers to the clay matrix improves the strain-sensing capability and the linearity of the response of the sensors with respect to normal bricks. Electromechanical tests on small-scale walls, each equipped with a smart brick made with different amount of stainless steel micro-fibers, have pointed out the capability of the smart brick doped with 0.25% of filler, to detect changes in strain conditions by providing a linear electrical output also when embedded into a structural element. Results obtained from the eccentric compression load tests with increasing intensity, performed on a middle-scale wall instrumented with seven 0.25% smart bricks, have demonstrated that the novel sensors are able to monitor variations in axial strain produced by the increase in the existing cracking pattern. Furthermore, numerical simulations with kriging interpolations have confirmed that data provided by smart bricks can be used to reconstruct the strain field map in order to understand which part of a structural element is the most stressed and critical. The kriging interpolator was also employed to assess the optimal smart-brick configuration for the detection of variations in axial strain of the middle-scale wall, demonstrating that the strain field map predicted with four smart bricks was capable to represent the strain condition of the structural element with an acceptable accuracy. Overall, reported results confirm that smart bricks represent a promising new sensing technology for the structural health monitoring of masonry buildings and that kriging interpolator can be an useful tool to reconstruct strain field maps based on smart bricks' measurements and to assess the optimal smart-brick deployment in a masonry element.

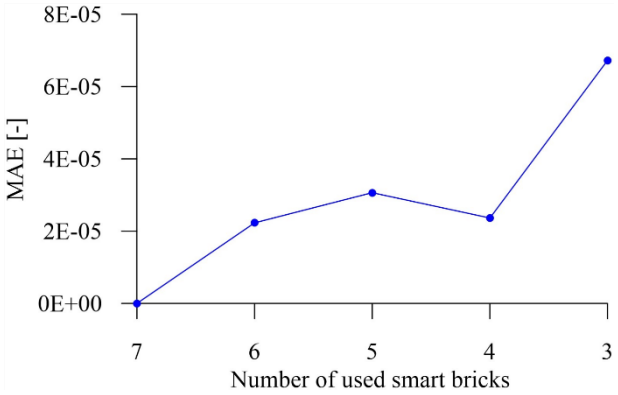

Figure 9. Mean Absolute Error (MAE) for strain filed maps reconstructed by varying the number of the considered smart bricks.

ACKNOWLEDGEMENTS

This work was supported by the Italian Ministry of Education, University and Research (MIUR) through the funded project of Relevant National Interest (PRIN) "SMART-BRICK: Novel strain-sensing nanocomposite clay brick enabling self-monitoring masonry structures" (Protocol no. 2015MS5L27).

REFERENCES

Carpinteri A., Lacidogna G., 2006. Damage monitoring of an historical masonry building by the acoustic emission technique. *Mater Struct.* **39**(2), pp. 161-167.

Coppola, L., Buoso, A., Corazza, F., 2011. Electrical Properties of Carbon Nanotubes Cement Composites for Monitoring Stress Conditions in Concrete Structures. *Applied Mechanics and Materials* **82**, pp.118-123.

Cressie, N., 1988. Spatial prediction and ordinary kriging, *Mathematical geology*, **20**(4), pp.405-421.

D'Alessandro, A., Meoni, A., Ubertini, F. 2018. Stainless Steel Microfibers for Strain-Sensing Smart Clay Bricks. *Journal of Sensors* **2018**; 2018(7431823)

De Lorenzis, L., DeJong, M., Ochsendorf, J., 2007. Failure of masonry arches under impulse base motion. *Earthquake Eng Struct Dyn.* **36**(14), pp. 2119-2136.

Downey, A., D'Alessandro, A., Baquera, m., García-Macías, E., Rolfes, D., Ubertini, f., Laflamme, S., Castro-Triguero, R., 2017. Damage detection, localization and quantification in conductive smart concrete structures using a resistor mesh model, *Engineering Structures*, **148**, pp. 924-935

Downey, A., D'Alessandro, A., Ubertini, F., Laflamme, S., Geiger, R., 2017. Biphasic DC measurement approach for enhanced measurement stability and multi-channel sampling of self-sensing multi-functional structural materials doped with carbon-based additives, *Smart Materials and Structures*, **26**(065008): 6.

Downey, A., D'Alessandro, A., Laflamme, S., Ubertini, F., 2017. Smart bricks for strain sensing and crack detection in masonry structures, *Smart Materials and Structures*, **27**(1), p.015009.

Formisano, A., Vaiano, G., Fabbrocino, F., Milani, G., 2018. Seismic vulnerability of italian masonry churches: the case of the nativity of blessed virgin mary in stellata of bondeno. *J Build Eng.* **20**, pp. 179-200.

García-Macías, E., Downey, A., D'Alessandro, A., Castro-Triguero, R., Laflamme, S., Ubertini, F., 2017. Enhanced lumped circuit model for smart nanocomposite cement-based sensors under dynamic compressive loading conditions, *Sens Actuators A Phys*, **260**, pp. 45-57.

Han, B., Ding, S., Yu, X., 2015. Intrinsic self-sensing concrete and structures: A review. *Measurements*, **59**, pp. 110-128.

Laflamme, S., Ubertini, F., Saleem, H., D'Alessandro, A., Downey, A., Ceylan, H., Materazzi, A.L., 2015. Dynamic Characterization of a Soft Elastomeric Capacitor for Structural Health Monitoring, *J. Struct. Eng*., **141**(8), 04014186.

Masciotta, M.-G., Ramos, L.F., Lourenço, P.B., 2017. The importance of structuralmonitoring as a diagnosis and control tool in the restoration process of heritage structures: a case study in portugal. *J Cultural Heritag,*.**27**, pp. 36-47.

Mosquera, V., Smyth, A.W., Betti, R., 2012. Rapid Evaluation and Damage Assessment of Instrumented Highway Bridges, *Earthq. Eng. Struc.* **41**(4), pp. 755-774.

Meoni, A., D'Alessandro, A., Cavalagli, N., Gioffré, M., Ubertini, F., 2019. Shaking table tests on a masonry building monitored using smart bricks: Damage detection and localizatiom, *Earthq. Eng. Struc.***48**(8) pp. 910-928.

Pisello, A.L., D'Alessandro, A., Sambuco, S., Rallini, M., Ubertini, F., Asdrubali, F., Materazzi, A.L., Cotana, F., 2017. Multipurpose experimental characterization of smart nanocomposite cement-based materials for thermal-energy efficiency and strain-sensing capability. *Sol Energy Mater Sol Cells*, **161**, pp. 77–88.

Rainieri, C., Song, Y., Fabbrocino, G., Markand, J.S., Shanov, V., 2013. CNT-cement based composites: Fabrication, self-sensing properties and prospective applications to structural health monitoring. In: Proceedings SPIE, fourth international conference on smart materials and nanotechnology in engineering 8793, pp. 10.

Saisi, A., Gentile, C., Guidobaldi, M., Xu, M., 2014. Dynamic monitoring and seismic response of a historic masonry tower. *Key Eng Mater*. **628**, pp. 55-60.